SINTEF
PROCEEDINGS
2

Proceedings of the 12th International Conference on Computational Fluid Dynamics in the Oil & Gas, Metallurgical and Process Industries

Progress in Applied CFD – CFD2017

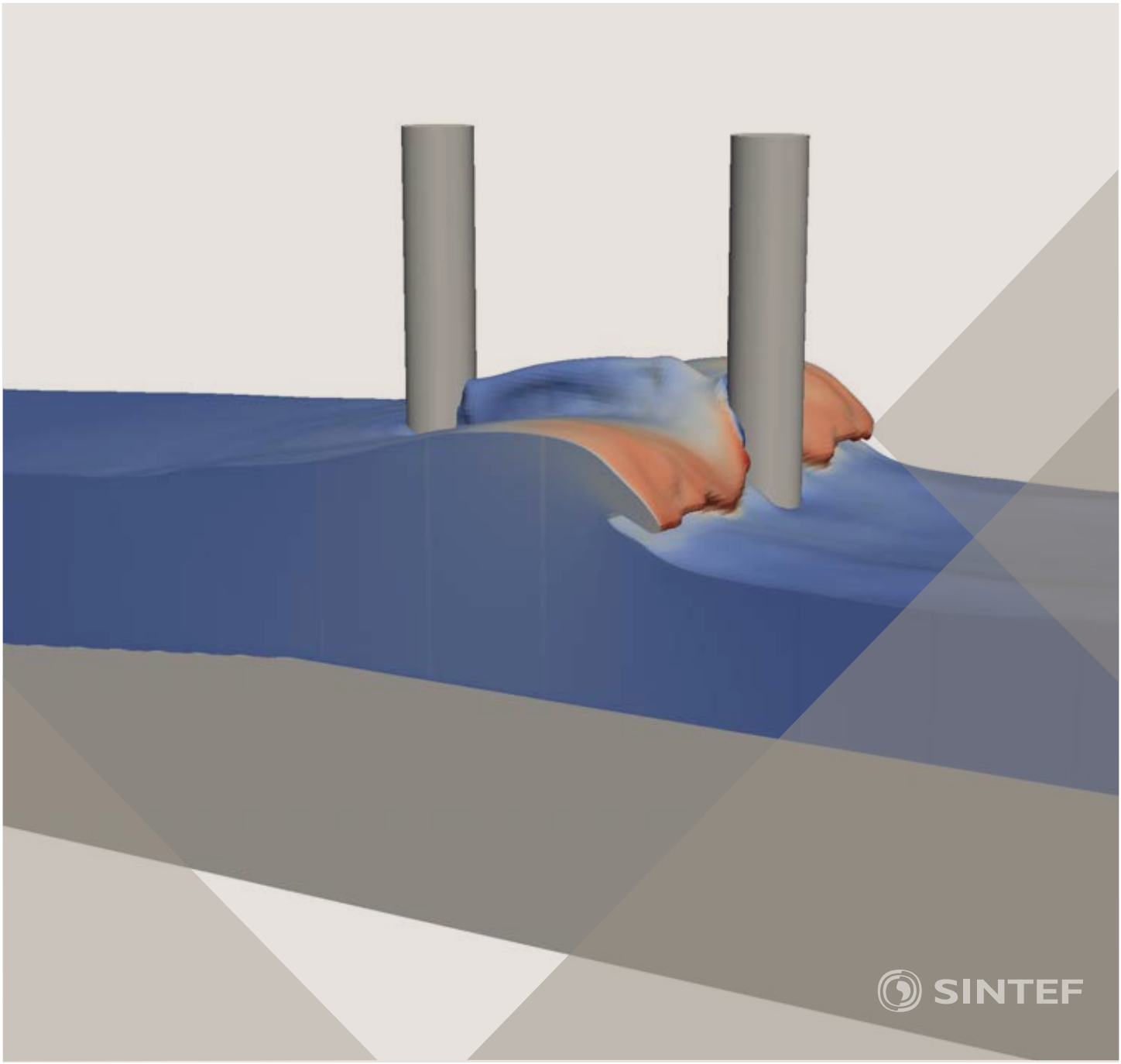

SINTEF Proceedings

Editors:
Jan Erik Olsen and Stein Tore Johansen

Progress in Applied CFD – CFD2017

Proceedings of the 12th International Conference on Computational Fluid Dynamics in the Oil & Gas, Metallurgical and Process Industries

SINTEF Academic Press

SINTEF Proceedings no 2
Editors: Jan Erik Olsen and Stein Tore Johansen
Progress in Applied CFD – CFD2017
Selected papers from 10th International Conference on Computational Fluid Dynamics in the Oil & Gas, Metallurgical and Process Industries

Key words:
CFD, Flow, Modelling

Cover, illustration: Arun Kamath

ISSN 2387-4295 (online)
ISBN 978-82-536-1544-8 (pdf)

SINTEF Academic Press
Address: Forskningsveien 3 B
PO Box 124 Blindern
N-0314 OSLO
Tel: +47 73 59 30 00
Fax: +47 22 96 55 08

www.sintef.no/byggforsk
www.sintefbok.no

SINTEF Proceedings
SINTEF Proceedings is a serial publication for peer-reviewed conference proceedings on a variety of scientific topics.
The processes of peer-reviewing of papers published in SINTEF Proceedings are administered by the conference organizers and proceedings editors. Detailed procedures will vary according to custom and practice in each scientific community.

PREFACE

This book contains all manuscripts approved by the reviewers and the organizing committee of the 12th International Conference on Computational Fluid Dynamics in the Oil & Gas, Metallurgical and Process Industries. The conference was hosted by SINTEF in Trondheim in May/June 2017 and is also known as CFD2017 for short. The conference series was initiated by CSIRO and Phil Schwarz in 1997. So far the conference has been alternating between CSIRO in Melbourne and SINTEF in Trondheim. The conferences focuses on the application of CFD in the oil and gas industries, metal production, mineral processing, power generation, chemicals and other process industries. In addition pragmatic modelling concepts and bio-mechanical applications have become an important part of the conference. The papers in this book demonstrate the current progress in applied CFD.

The conference papers undergo a review process involving two experts. Only papers accepted by the reviewers are included in the proceedings. 108 contributions were presented at the conference together with six keynote presentations. A majority of these contributions are presented by their manuscript in this collection (a few were granted to present without an accompanying manuscript).

The organizing committee would like to thank everyone who has helped with review of manuscripts, all those who helped to promote the conference and all authors who have submitted scientific contributions. We are also grateful for the support from the conference sponsors: ANSYS, SFI Metal Production and NanoSim.

Stein Tore Johansen & Jan Erik Olsen

Organizing committee:

Conference chairman: Prof. Stein Tore Johansen
Conference coordinator: Dr. Jan Erik Olsen
Dr. Bernhard Müller
Dr.Sigrid Karstad Dahl
Dr.Shahriar Amini
Dr.Ernst Meese
Dr.Josip Zoric
Dr.Jannike Solsvik
Dr.Peter Witt

Scientific committee:

Stein Tore Johansen, SINTEF/NTNU
Bernhard Müller, NTNU
Phil Schwarz, CSIRO
Akio Tomiyama, Kobe University
Hans Kuipers, Eindhoven University of Technology
Jinghai Li, Chinese Academy of Science
Markus Braun, Ansys
Simon Lo, CD-adapco
Patrick Segers, Universiteit Gent
Jiyuan Tu, RMIT
Jos Derksen, University of Aberdeen
Dmitry Eskin, Schlumberger-Doll Research
Pär Jönsson, KTH
Stefan Pirker, Johannes Kepler University
Josip Zoric, SINTEF

CONTENTS

HIGH TEMPERATURE FLUIDIZATION – INFLUENCE OF INTER-PARTICLE FORCES ON FLUIDIZATION BEHAVIOR

Milan MIHAJLOVIC[1] , Ivo ROGHAIR[1*], Martin van Sint ANNALAND[1]

[1] Eindhoven University of Technology, 5600 MB Eindhoven, NETHERLANDS

* E-mail: I.Roghair@tue.nl

ABSTRACT

Recent experiments have shown an influence of temperature on the minimum fluidization conditions in gas-solid fluidized beds, even when the gas phase density and viscosity were kept constant (Campos Velarde et al., 2016). Correlations that are available in the open literature, for predicting the minimum fluidization velocity and the bed voidage at minimum fluidization conditions at elevated temperatures, fail to describe their experimental data, in particular how the bed porosity at incipient fluidization conditions is changing with temperature.

It is hypothesized that at higher temperatures inter-particle forces play an important role in this phenomenon. Inter-particle forces, specifically van der Waals forces, are known to be important in the fluidization of very fine powders, and may incur detrimental effects on the process such as the formation of particle agglomerates or reduced particle mixing. However, the experimental results by Campos Velarde et al. (2016) have indicated that such forces may also become important during the fluidization of larger particles at increased temperatures. In this work, we characterize the effects of inter-particle forces using simulations with a Discrete Particle Model (DPM).

DPM is an Euler-Lagrange type model with a discrete description of the solids phase and a continuous description of the gas phase. The motion of each individual particle is tracked and described with Newton's second law, with van der Waals forces used to describe the inter-particle forces. Van der Waals forces are described with a Hamaker constant, which depends on the particle material and fluidization gas properties and may depend on temperature (Castellanos et al., 2003). Particle-particle interactions are dealt with using a soft-sphere collision model, which allows multiple simultaneous contacts between several pairs of particles. The gas phase is described with a set of volume-averaged Navier-Stokes equations, and full two-way coupling between the phases is implemented.

In this work we investigate the influence of the inter-particle forces (by variation of the Hamaker constant) on the minimum fluidization velocity (U_{mf}) and the bed porosity at minimum fluidization (ε_{mf}), and relate the effects to the dominating phenomena prevailing at high-temperature fluidization.

Keywords: Discrete Particle Model, fluidized beds, minimum fluidization, interparticle forces.

NOMENCLATURE

Greek Symbols

ρ density, [kg/m^3].
ε porosity, [-].
μ dynamic viscosity, [kg/m.s].
τ viscous stress tensor, [kg/m s^2].
β inter-phase momentum exchange coefficient, [-].
ω rotational velocity, [rad/s].
ϕ sphericity, [-].

Latin Symbols

Ar Archimedes number, [-].
d particle diameter, [m].
$\mathbf{F}$ force, [N].
g gravitational acceleration, [m/s^2].
H Hamaker constant, [J].
I moment of inertia, [kg m^2].
K slope, [m/s^2].
m mass, [kg].
N_{part} number of particles, [-].
p pressure, [Pa].
Re Reynolds number, [-].
$\mathbf{r}$ particle position, [m].
r particle radius, [m].
S inter-surface distance between two spheres, [m]
$\mathbf{T}$ torque, [N m].
t time, [s].
$\mathbf{u}$ velocity, [m/s].
U_0 superficial gas velocity, [m/s].
v particle velocity, [m/s].
V volume, [m^3].

Sub/superscripts

0 initial state
a particle index
g gas phase.
p particle phase.
cont contact forces.
vdW van der Waals forces.
mf minimum fluidization point
mb minimum bubbling point

INTRODUCTION

Fluidized bed reactors are often used in the chemical process industry. Due to their sheer size, many studies have been and are being performed to optimize the operation of these reactors. Most industrial processes using fluidized beds are operated at reactive conditions, i.e. at elevated temperatures (Kunii and Levenspiel, 1991). Research has shown that operation at elevated temperature has an effect on the bed voidage and minimum fluidization velocity (Lettieri et al., 2001). However, there is an ongoing debate on the mechanism by which the temperature influences the fluidization process.

Since the early work by Geldart (1972), we know that different particle classes show very different fluidization behaviour even at ambient conditions. The boundaries between the different classes change at higher temperatures (Botterill et al., 1982). For instance, Botterill et al. (1982) and Lettieri et al. (2001) showed that particles that are originally classified as one Geldart type can change their fluidization characteristics to those belonging to another Geldart type with increasing temperature. One possible explanation for these changes in fluidization behaviour, according to Lattieri and Botterill, is that at high temperatures the gas phase properties (i.e. density and viscosity) change. However, other research suggests that also inter-particle forces (IPF) can have an important additional influence (Baerns (1966), Formisani et al. (1998)). Although the influence of the gas properties and IPFs occurs simultaneously during fluidization at elevated temperatures, researchers have debated about the relative contributions of these phenomena at different conditions. For example, Shabanian (2013) and Baerns (1966) have found that IPFs have a significant role using Geldart C type particles, whereas for Geldart B and D not much influence of IPFs were found. For Geldart A type particles, the debate is still ongoing.

Numerical analysis was performed in different studies in order to investigate the influence of the van der Waals (denoted as vdW) forces on the fluidization behaviour. Ye et al. (2004) and Kobayashi et al. (2006) performed an analysis on the fluidization of Geldart A type particles including vdW forces between adjacent particles. Ye et al. (2004) specifically examined the influence of the Hamaker constant on the fluidization behaviour. Results showed, for example, that for higher values of the Hamaker constant, Geldart A particles can exhibit the fluidization behaviour of Geldart C type particles. In their study, the value of the Hamaker constant was chosen with the objective to demonstrate the influence, but the value was not directly related to actual particle properties. In this work, we adopt a similar approach, where we extend the study to Geldart B type particles.

In a recent study done by Campos Velarde et al. (2016), a novel experimental approach was used for high temperature fluidization. The authors have carried out experiments where fluidization was performed with two different gas mixtures that possessed the same properties (density and viscosity) at different temperatures. It was shown that these two cases show different fluidization behaviour. This has lead the authors to suggest that IPFs could be the reason behind the observed phenomena.

In the work of Castellanos (2003) it is shown that the Hamaker constant is dependent on temperature which indicate that the magnitude of the IPFs will also change with temperature. This work gives a first look on how the change of IPFs could influence the fluidization.

Specifically, this work uses DEM simulations to show the influence of the vdW forces via the Hamaker constant on the minimum fluidization conditions (U_{mf} and ε_{mf}) and average particle circulation patterns of Geldart A and Geldart B particles.

MODEL DESCRIPTION

The model used in this work originates from the work of Hoomans et al. (1996), Ye et al. (2004), and Tan et al. (2014). The gas flow is modelled by the volume-averaged Navier–Stokes equations

$$\frac{\partial(\varepsilon\rho_g)}{\partial t} + \nabla\cdot\left(\varepsilon\rho_g\mathbf{u}\right) = 0 \tag{1}$$

$$\frac{\partial(\varepsilon\rho_g\mathbf{u})}{\partial t} + \nabla\cdot\left(\varepsilon\rho_g\mathbf{u}\mathbf{u}\right) = -\varepsilon\nabla p - \mathbf{S}_p - \nabla\cdot(\varepsilon\tau) + \varepsilon\rho_g\mathbf{g} \tag{2}$$

where ε is the porosity, and ρ_g, $\boldsymbol{u}$, τ and p are the density, velocity, viscous stress tensor, and pressure of the gas phase, respectively. The source term $\mathbf{S}_p$ is defined as:

$$\mathbf{S}_p = \frac{1}{V}\int\sum_{a=0}^{N_{part}}\frac{\beta V_a}{1-\varepsilon}(\mathbf{u}-\mathbf{v}_a)\mathcal{S}(\mathbf{r}-\mathbf{r}_a)dV \tag{3}$$

Note that V is the volume of the fluid cell, V_a the volume of particle, $\boldsymbol{v}_a$ the particle velocity, $\mathbf{r}_a$ is the position of a particle, N_{part} the number of particles and β is the inter-phase momentum exchange coefficient. The δ-function ensures that the drag force acts as a point force at the (central) position of a particle. The distribution function for mapping the properties from the Lagrangian particle positions to the Eulerian computational grid and vice versa is implemented in a straightforward manner through volume-weighing techniques (Hoomans et al., 1996), which is often used when the volume of the smallest computational cell for the fluid is (much) larger than the volume of a particle. The integration calculates the total drag force between the gas phase and the particles in a computational cell.

For the solids phase, the motion of each particle is described with Newton's second law of motion. The translational motion of a single particle with mass m_a and volume V_a is computed with the following equation:

$$m_a\frac{d^2\mathbf{r}_a}{dt^2} = \mathbf{F}_{cont,a} + F_{vdw,a} + \frac{V_a\beta}{1-\varepsilon}(\mathbf{u}-\mathbf{v}_a) - V_a\nabla p + m_a g \tag{4}$$

The forces on the right hand side of Equation (4) represent the contact force, vdW force, drag force, pressure gradient and gravity respectively. The rotational force balance is given by

$$I_a\frac{\partial\omega_a}{\partial t} = \mathbf{T}_a \tag{5}$$

where $\boldsymbol{T}_a$ is the torque, I_a the moment of inertia, and ω_a the rotational velocity.

The contact force between two particles (or a particle and a sidewall) is calculated by use of the soft-sphere model developed by Cundall and Strack (1979). In this model, a linear-spring and a dashpot are used to formulate the normal contact force, while a linear-spring, a dashpot and a slider are used to compute the tangential contact force, where the tangential spring stiffness is $\frac{2}{7}^{\text{th}}$ of the normal spring stiffness.

In order to resolve the time-dependent motion of particles and the dynamics of the gas phase, two different time steps are used to solve the particle collisions and the Navier–Stokes equations. The time step in the soft-sphere model depends on the duration of a contact and should be sufficiently small to make sure that the contact lasts for a certain number of time steps. Doing so helps to avoid problems concerning energy conservation due to the numerical integration, which is inevitable in the soft-sphere model. The time step for the particle phase can calculated from:

$$\Delta t = \frac{1}{K_N} t_{contact,n} = \frac{1}{K_N} \sqrt{\frac{\pi^2 + (\ln e_n)^2}{k_n / m_{ab}}} \qquad (6)$$

where K_N is the minimum number of steps during one contact and normally in the range of 15–50. Using the normal stiffness k_n determined from the Youngs modulus will result a very small time step which will require a large computation time. It has been found (Tsuji, 1993), however, that one can set k_n to a lower value than the one derived from material properties without loss of accuracy for gas–solid fluidized beds. At the same time, k_n should be a value sufficiently large so that the maximum overlap between particles is below 1% of the particle diameter to ensure that the computed hydrodynamics are not affected. As shown in Table 1, k_n is set to a value such that at the very least 15 particle time steps are taken to evaluate a single contact, which gives 1×10^{-6} s as the time step for the selected particle phase in this work.

To calculate the inter-particle vdW forces, we adopt the Hamaker scheme (Israelachvili, 1991):

$$F_{vdw,ab} = \frac{H}{3} \frac{2r_1 r_2 (S + r_1 + r_2)}{[S(S + 2r_1 + 2r_2)]^2} \times \left[\frac{(S + 2r_1 + 2r_2)}{(S + r_1 + r_2)^2 - (r_1 - r_2)^2} - 1 \right]^2 \qquad (7)$$

where, S is the inter-surface distance between two spheres, H the Hamaker constant, and r_1 and r_2 the radii of the two spheres, respectively. However, Eq. (7) exhibits an apparent numerical singularity that the vdW interaction diverges if the distance between two particles approaches zero. In reality, such a situation will never occur, because of the short-range repulsion between particles. In the present model, we have not included this repulsion, however, we can avoid the numerical singularity by defining a cut-off (maximal) value of the vdW force between two spheres. In the simulations only particle-particle vdW forces have been used, no particle-wall interactions other than collisions have been considered.

Numerical simulations

Input parameters

In order to investigate the influence of vdW forces we consider two systems: one with Geldart A type particles with diameter of 100 μm and a density of 900 kg/m^3, and a second one with Geldart B type particles with diameter of 500 μm and a density of 2525 kg/m^3. Input parameters used for both systems are shown in Table 1.

Table 1: Parameters used in simulation for vdW forces.

Particle type	Geldart A	Geldart B	
Number of particles	7000	12000	
Particle diameter, d_p	100	500	μm
Particle density, ρ	900	2525	kg/m^3
Normal restitution coefficient, e_n	0.9	0.97	-
Tangential restitution coefficient, e_t	0.9	0.33	-
Friction coefficient, μ_t	0.3	0.1	-
Normal spring stiffness, k_n	420	7000	N·m
Tangential spring stiffness, k_t	120	2000	N·m
CFD time step	1×10^{-5}		s
Particle time step, Δt	1×10^{-6}		s
Minimum interparticle distance, S_o	0.4		nm
System height, *Zmax*	15	45	mm
System width, *Xmax*	2	10	mm
System depth, *Ymax*	1	10	mm
CFD grid height, Δx	250	1250	μm
CFD grid width, Δy	250	1250	μm
CFD grid depth, Δz	250	1250	μm
Shear viscosity of gas, μ	1.8×10^{-5}		Pa·s
Gas temperature, T	293		K
Hamaker constant, H	$10^{-19}/10^{-20}/10^{-21}/10^{-22}$		J

Procedure and initial condition

The Hamaker constant is known to be dependent on particle properties and the gas properties between the particles (Lefèvre (2009), Hamaker (1937)). In this research the primary goal is to investigate how the vdW forces affect the minimum fluidization conditions, so a value range of the Hamaker constant will be taken from 10^{-19} down to 10^{-22} J. All simulations start by fluidizing the particles by a relatively large gas velocity for 2 s (Geldart A at 0.04 m/s; Geldart B at 0.45 m/s), and after the initial fluidization the gas supply is switched off causing the particles to drop down to form a packed bed. After a short settling period, the superficial gas velocity U_0 is set to increase slowly and linearly in time:

$$U_0 = Kt \qquad (8)$$

Here the rate constant K is 0.03 m/s^2, which is by Ye et al. (2005) optimal in the sense that this yields a reasonable speed-up compared to the step-wise method, where the deviation in the predicted pressure drop and bed height is minimal (again compared to the results from the step-wise method).

Simulation results

Geldart A type particles

The main focus of this part of the study is to investigate the influence of vdW forces on the minimum fluidization velocity. A number of snapshots of the simulations from a central slice of the bed (using no vdW forces, and Hamaker constants in the range of 10^{-21} to 10^{-19} J) are shown in Figure 1. We observe that bubble formation is suppressed for higher Hamaker constants.

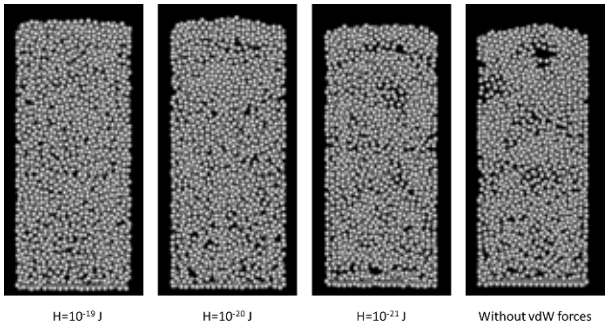

Figure 1: Snapshots from simulations showing the influence of the Hamaker constant on fluidization. Simulations were performed for Geldart A particles with the same superficial gas velocity.

From Figure 2, showing the pressure drop over the bed as a function of the superficial gas velocity, we can draw the quantitative conclusion that vdW forces have a negligible influence on U_{mf}. The biggest influence is observed during the transition from a fixed bed to the fluidized bed. Simulations that include vdW forces in the Δp-U_{mf} graph show a more smooth transition from packed bed state towards the fluidized state as the Hamaker constant increases. One explanation for this behaviour would be that with a higher Hamaker constant particles form channels and clusters and by doing so allow gas to pass through the bed (Ye et al., 2004). We can take a look at snapshots from simulations presented in the Appendix (Figure 7), showing the gas density on a slice in the middle of the bed at the specific times. These snapshots show that for $H = 10^{-19}$ and 10^{-20} J there is a longer homogeneous fluidization, which may be due to formed small clusters or channels. A further investigation on the emergence, whereabouts and possibly disintegration of these structures (channels and clustered particles) will be reported in a future work. An algorithm that can accurately locate such structures is under development.
Values of U_{mf} determined from the simulations for different Hamaker constants are given in Table 2:

Table 2: Determined Umf for various Hamaker constants

Hamaker constant H [J]	Determined U_{mf} [m/s]
0	3.94×10^{-3}
10^{-22}	3.94×10^{-3}
10^{-21}	4.01×10^{-3}
10^{-20}	4.07×10^{-3}
10^{-19}	3.8×10^{-3}

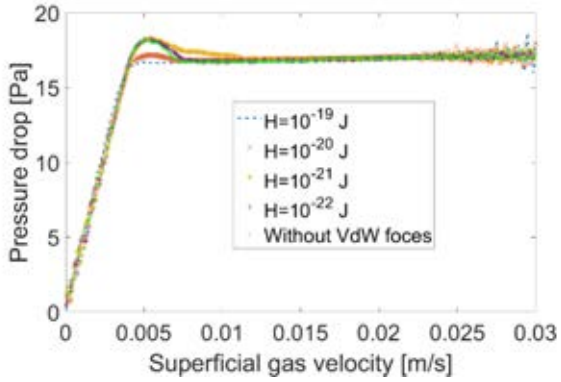

Figure 2: Influence of the Hamaker constant on the pressure drop as a function of the gas velocity for Geldart A particles.

We conclude that these changes are unimportant and that the biggest influence of the Hamaker constant is the reduction of the hysteresis and a slight decrease in the Δp-U_{mf} slope of the homogeneous part of the fluidization. This effect could be explained in two ways; firstly, a reason could be a numerical artefact due to the soft sphere method that was employed in the DPM code for the particle collisions. As indicated in the model description, we assume a certain value of the spring stiffness that will avoid particle overlap exceeding 1% of their particle diameter during the simulation. Although for all the other types of simulation with fluidized beds this maximum overlap yielded satisfactory results, for simulations with higher Hamaker constants this maximally allowed overlap of 1% could still be too large. We can take a look at snapshots from simulations presented in the Appendix (Figure 9), showing the particle overlap for different Hamaker constants at the same gas velocity. Further investigation is ongoing on this topic to investigate whether it is necessary reduce the maximally allowed overlap. The second explanation lies in a possible existence of clusters and channels that would allow gas bypass which would reduce the pressure drop.
Compared with work of Ye et al. (2004), our conclusions are matching well, the biggest difference is that their approach for determining U_{mf} was a step-wise method of increasing the gas velocity instead of a continuous incrementing gas flow rate.
The values determined from the simulations are slightly higher in comparison to the values calculated using the basic Ergun equation (Eq 9) with the bed porosity taken from our simulations.

$$\frac{1.75}{\varepsilon_{mf}^3 \phi}(\mathrm{Re}_{mf})^2 + \frac{150(1-\varepsilon_{mf})}{\varepsilon_{mf}^3 \phi^2}(\mathrm{Re}_{mf}) = Ar \qquad (9)$$

where the Reynolds number at minimum fluidization and the Archimedes number are defined as

$$\mathrm{Re}_{mf} = \frac{\rho_g d_p U_{mf}}{\mu_g} \qquad (10)$$

$$Ar = \frac{(\rho_p - \rho_g) g \rho_g (d_p)^3}{(\mu_g)^2} \qquad (11)$$

Substituting the simulation data into these equations we obtain a value for the minimum fluidization velocity of 0.0034 m/s for ε_{mf}= 0.4. This value is not significantly different from the values obtained from Figure 2.
Simulations including Van der Waals forces show a clear influence on the average bed porosity (Figure 3). The bed porosity for increasing Hamaker constant is increasing, however, we observe for the largest Hamaker constant that the bed height and porosity are lower than the case without vdW forces. As noted before, this effect could be due to the soft sphere method.
The minimum bubbling velocity U_{mb} can be determined by using a combination of the snapshots of the bed porosity and from Δp-U_0 graph. For all cases, bubbles start to appear at around 0.023 m/s, which is lower than the value reported in Ye et al.'s (2004) work. It is important to mention that our simulations were performed in 3D, whereas Ye et al. (2004) used 2D simulations.

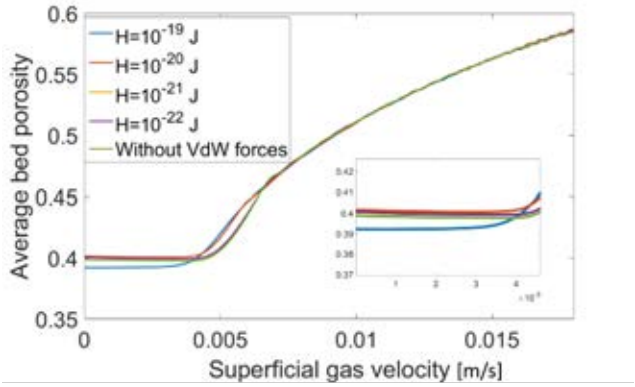

Figure 3: Average bed porosity as a function of the superficial gas velocity.

The influence of van der Waals forces on the time-averaged solids velocity is shown in Figure 8 in the Appendix.
The time averaged solids velocities were plotted for $H = 10^{-19/20/21}$ J at gas velocities 0.004 m/s and 0.014 m/s. For all the cases the circulation patterns follow the anticipated profile with solids flowing upwards in the centre of the bed and downwards near the walls of the column. For cases with the superficial gas velocity close to the minimum velocity, the solids circulation rate is somewhat reduced for cases with higher Hamaker constants, as expected. At higher superficial gas velocities this effect is similar, but somewhat less pronounced.

Geldart B type particles

As a first step in the investigation of high-temperature fluidization of Geldart B type particles, we have examined the minimum fluidization conditions. Compared to Geldart A particles, a similar effect on U_{mf} was observed also for Geldart B particles. For higher Hamaker constants, the superficial gas velocity at incipient fluidization conditions is slightly higher (see Figure 4). However, we do not observe a decrease in the minimum fluidization gas velocity for H=10^{-19} J, but found a significant increase in the minimum fluidization velocity. The values for the minimum fluidization velocity determined from the simulation results are given in Table 3:

Table 3: Determined U_{mf} for various Hamaker constants

Hamaker constant H [J]	Determined U_{mf} [m/s]
0	0.2224
10^{-22}	0.2274
10^{-21}	0.2277
10^{-20}	0.2321
10^{-19}	0.2885

When calculating U_{mf} using Ergun's equation with characteristics for Geldart B particles and with the porosity from simulations (ε_{mf}= 0.4), we find 0.226 m/s, which is very close to the simulated values.

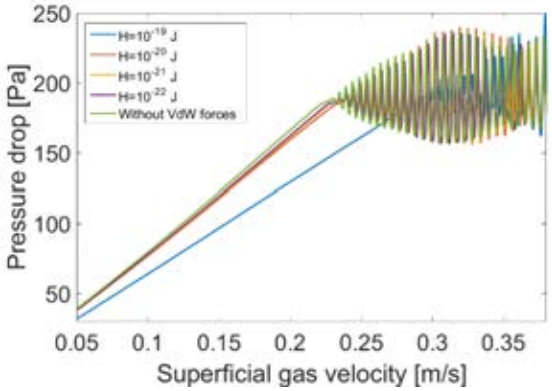

Figure 4: Influence of the Hamaker constant on the pressure drop vs. the superficial gas velocity for Geldart B particles.

For the time-averaged bed porosity a slightly different behaviour was observed compared to our findings for Geldart A particles. It was also found that by increasing the gas velocity the bed porosity tends to increase (Figure 5). However, for a very high Hamaker constant, the bed porosity was larger than for the case without vdW forces, which is clearly different from the Geldart A simulations.

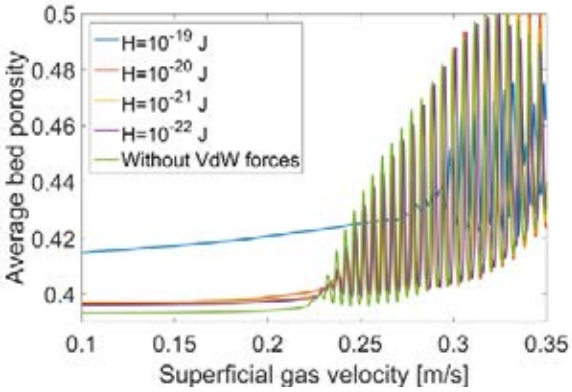

Figure 5: Bed porosity as a function of the gas velocity, influence of the Hamaker constant on the bed compaction.

A possible reason for this behaviour we can find in the fact that simulations start by fluidizing the particles with a relatively large gas velocity for 2 s, after which the gas flow is switched off and the particles drop down to form the initial situation before the velocity starts to increase linearly in time. By doing so, the particles in the simulations with a larger Hamaker constant tend to form clusters that affect the overall bed porosity with the formation of larger voids. In comparison, the case without vdW forces shows that particles have been

distributed more uniformly over the bottom of the reactor (Appendix, Figure 10) resulting in a higher overall bed porosity.

Similar to the results for Geldart A particles, the average overlap is higher for the case with a stronger Hamaker constant (Figure 6) and this needs to be further investigated.

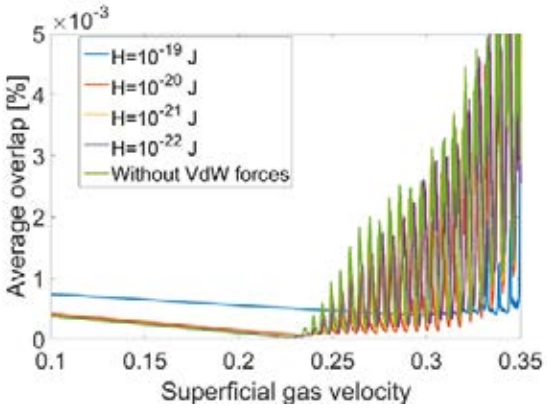

Figure 6: Average overlap between particles during the simulations, the effect of the Hamaker constant on the bed porosity may be related to the increased particle overlap.

In a future work a more detailed comparison will be carried out between the experiments at high temperatures and DPM simulations including vdW forces.

CONCLUSIONS

The main conclusions are:

1. For both Geldart A and Geldart B particles vdW forces increase the minimum fluidization bed porosity (increased bed height).
2. For higher Hamaker constants Geldart B particles tend to form unstable channels and clusters.
3. The effect of the maximum particle overlap has to be further investigated. The current maximum allowed overlap may not suitable for the cases of the strongest considered Hamaker constants, where the average particle overlap is higher.

ACKNOWLEDGMENTS

The authors wish to thank the European Commission for supporting this work as part of the research project "Intensified by Design platform for the intensification of processes involving solids handling", IbD®, under the H2020 SPIRE programme (SPIRE-08-2015-680565).

REFERENCES

BAERNS, M., (1966), "Effect of Interparticle Adhesive Forces on Fluidization of Fine Particles", *Ind. Eng. Chem. Fundamen.*, **5 (4),** 508–516

BOTTERILL, J.S.M., TEOMAN, Y., YÜREGIR, K.R., (1982), "The Effect of Operating Temperature on the Velocity of Minimum Fluidization, Bed Voidage and General Behavior", *Powder Technology*, **31**, 101 – 110

CAMPOS VELARDE, I., GRIM, R., GALLUCCI, F., VAN SINT ANNALAND, M., (2016), "Influence of Temperature on Minimum Fluidization Properties of Gas-Solid Fluidized Beds", *Powder Technology*, Submitted.

CASTELLANOS, A. J., GARCIA-SUCRE, M., URBINA-VILLALBA G., (2003), "Temperature dependence of Hamaker constants for fluorocarbon compounds" *The Journal of Physical Chemistry B*, ***107,*** 8532-8537

CUNDALL, P.A., STRACK, O.D., (1979), "A discrete numerical model for granular assemblies", *Geotechnique,* **29**, 47.

FORMISANI, B., GIRIMONTE, R., MANCUSO, L., (1998) "Analysis of the fluidization process of particle beds at high temperature", *Chemical Engineering Science,* **53(5)**, 951–961

GELDART, D. (1972), "The Effect of Particle Size and Size Distribution on the Behaviour of Gas-Fluidised Beds", *Powder Technology,* **6,** 201-215

GELDART, D. (1973), "Types of gas fluidization", *Powder Technology,* **7**, 285-292

HAMAKER, H.C., (1937) "The London – van der Waals attraction between spherical particles", *Physica,* **4(10)**, 1058–1072.

HOOMANS, B.P.B., KUIPERS, J.A.M., BRIELS, W.J., VAN SWAAIJ, W.P.M., (1996) "Discrete particle simulation of bubble and slug formation in a two-dimensional gas-fluidised bed: a hard-sphere approach" *Chemical Engineering Science,* **51**, 99–118.

ISRAELACHVILI, J., (1991) "Intermolecular and Surface Forces", *Academic Press, London*

KOBAYASHI, T., MUKAI, T., KAWAGUCHI, T., TANAKA T., TSUJI Y., (2006), "DEM Analysis on Flow Patterns of Geldart's Group A Particles in Fluidized Bed-Effect of Adhesion and Lubrication Forces", *Journal of the Society of Powder Technology, Japan,* **43**, 737-745

KUNII, D., LEVENSPIEL, O., (1991.) "Fluidization engineering", Butterworth-Heinmann, London

LEFÈVRE, G., JOLIVET, A., (2009), "Calculation of Hamaker constants applied to the deposition of Metallic oxide particles at high temperature", *Proceedings of International Conference on Heat Exchanger Fouling and Cleaning VIII*

LETTIERI, P., NEWTON, D., YATES, J.G., (2001), "High temperature effects on the dense phase properties of gas fluidized beds", *Powder Technology,* **120**, 34–40

SHABANIAN, J., FOTOVAT, F., CHAOUKI, J., BOUFFARD, J., (2013) "Fluidization Behavior in a Gas- Solid Fluidized Bed with Thermally Induced Inter-Particle Forces" *10th International Conference on Circulating Fluidized Beds and Fluidization Technology - CFB-10", Eds, ECI Symposium Series, Volume RP7*

SEVILLE, J.P.K., WILLETT, C.D., KNIGHT P.C., (2000), "Interparticle forces in fluidisation: a review", *Powder Technology.* **113**, 261–268

SUBRAMANI, H.J., BALAIYYA, M.B.M., MIRANDA, L.R., (2007), "Minimum fluidization velocity at elevated temperatures for Geldart's group-B powders", *Experimental Thermal and Fluid Science,* **32**, 166–173

TAN, L., ROGHAIR, I., VAN SINT ANNALAND, M., (2014) "Simulation study on the effect of gas permeation on the hydrodynamic characteristics of membrane-assisted micro fluidized beds", *Applied Mathematical Modeling,* **38**, 4291-4307

TSUJI, Y., KAWAGUCHI, T., TANAKA, T., (1993) "Discrete particle simulation of two-dimensional fluidized bed", *Powder Technology,* **77**, 79–87.

YE, M., VAN DER HOEF, M.A., KUIPERS, J.A.M., (2004) "A numerical study of fluidization behavior of Geldart A particles using a discrete particle model", *Powder Technology,* **139**, 129-139

YE, M., VAN DER HOEF, M.A., KUIPERS, J.A.M., (2005) "The effects of particle and gas properties on the fluidization of Geldart A particles", *Chemical Engineering Science* **60**, 4567 – 4580

APPENDIX

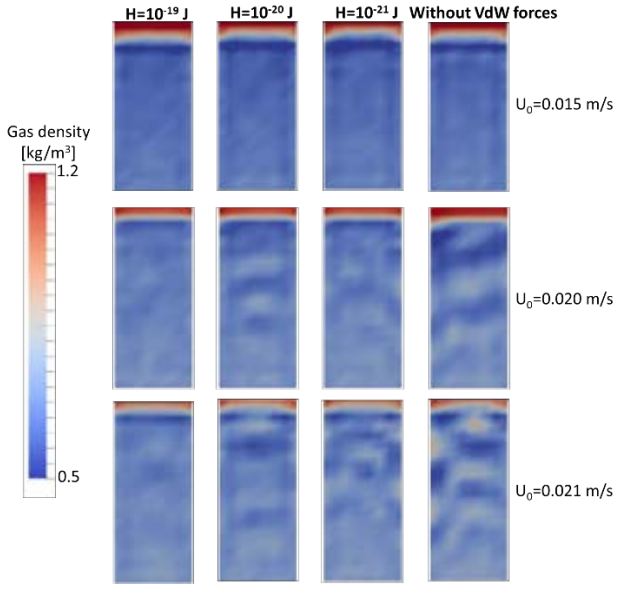

Figure 7: Gas density distribution in the bed of Geldart A particles.

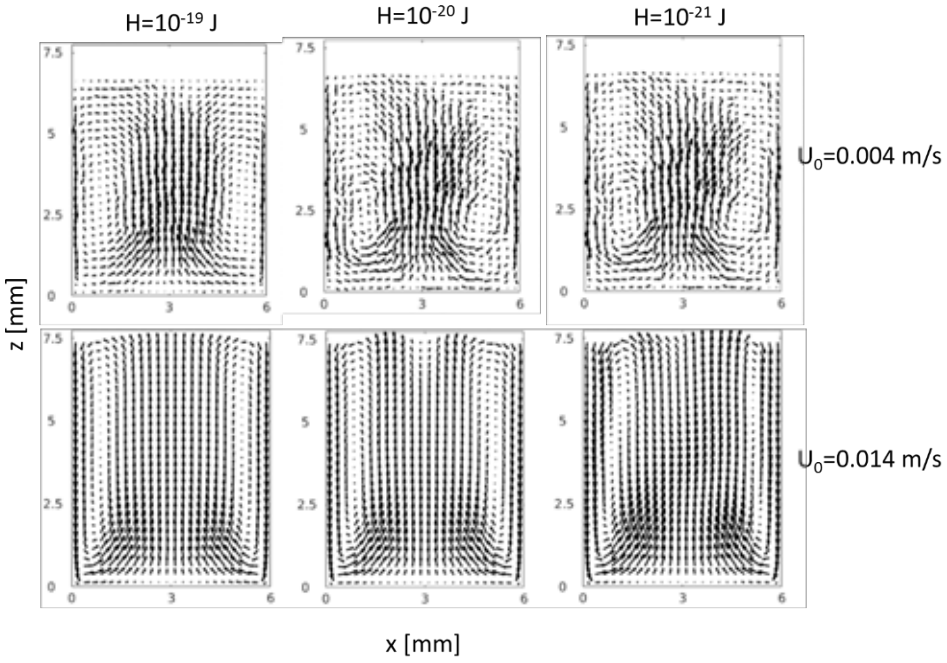

Figure 8: Average particle velocity for different Hamaker constants. Geldart A particles.

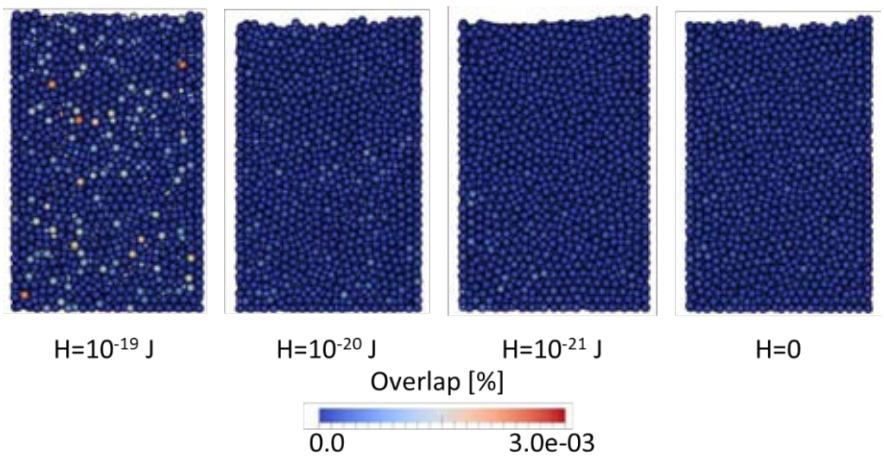

Figure 9: Overlap between the particles for different Hamaker constants at U_0=0.0035 m/s

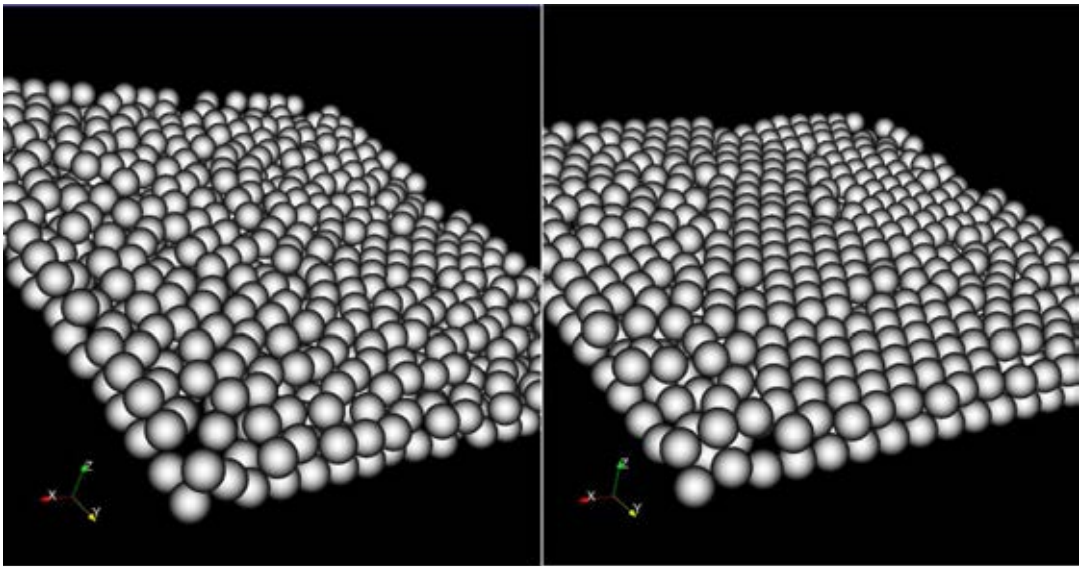

Figure 10: Slice of the bottom of the bed after the particle drop. Influence of vdW forces on fixed bed.